Hindawi
Geofluids
Volume 2017, Article ID 6059142, 14 pages
https://doi.org/10.1155/2017/6059142

WILEY | Hindawi

Research Article

Evaluating Reservoir Risks and Their Influencing Factors during CO_2 Injection into Multilayered Reservoirs

Lu Shi, Bing Bai, Haiqing Wu, and Xiaochun Li

State Key Laboratory of Geomechanics and Geotechnical Engineering, Institute of Rock and Soil Mechanics, Chinese Academy of Sciences, Wuhan 430071, China

Correspondence should be addressed to Lu Shi; shilu.whrsm@qq.com

Received 13 March 2017; Revised 18 July 2017; Accepted 14 August 2017; Published 1 October 2017

Academic Editor: Tianfu Xu

Wellbore and site safety must be ensured during CO_2 injection into multiple reservoirs during carbon capture and storage projects. This study focuses on multireservoir injection and investigates the characteristics of the flow-rate distribution and reservoir-risk evaluation as well as their unique influences on multireservoir injection. The results show that more CO_2 enters the upper layers than the lower layers. With the increase in injection pressure, the risks of the upper reservoirs increase more dramatically than those of the low reservoirs, which can cause the critical reservoir (CR) to shift. The CO_2 injection temperature has a similar effect on the injection flow rate but no effect on the CR's location. Despite having no effect on the flow-rate distribution, the formation-fracturing pressures in the reservoirs determine which layer becomes the CR. As the thickness or permeability of a layer increases, the inflows exhibit upward and downward trends in this layer and the lower layers, respectively, whereas the inflows of the upper layers remain unchanged; meanwhile, the risks of the lower layer and those of the others decrease and remain constant, respectively. Compared to other parameters, the reservoir porosities have a negligible effect on the reservoir risks and flow-rate distributions.

1. Introduction

Carbon capture and storage (CCS) is widely recognized as an effective approach for greatly reducing CO_2 levels in the atmosphere [1–5]. Many CCS projects have been conducted worldwide, including the Sleipner project [6, 7] in Norway, the Weyburn project in Canada [8], the Otway Pilot project in Australia [9], the In Salah project in Algeria [6], and the Shenhua CCS demonstration project in China [10]. Wellbore and site safety must be ensured in all fluid injection projects [11, 12]. In many CCS projects, particularly those with large-scale CO_2 injection, multiple reservoirs are employed for simultaneous injection to achieve a preset injection target amount of CO_2 (see [13–16]). Layers of caprocks and reservoirs are sequentially spaced to form multiple suits of cap rock-reservoir combinations, which significantly increase the complexity of fluid migrations [14]. A mature design methodology for safe and effective CO_2 injection through deep wellbores requires an in-depth understanding of the reservoir performance and safety and their influencing factors in terms of CO_2 injection.

The injection of CO_2 with multiple layers differs considerably from single-layer injection in several respects. First, safe injection requires that the pressure in each reservoir does not exceed the maximum allowable value. Second, the flow rate of each reservoir is unknown in advance of the initial injection. Third, the most dangerous reservoir, based on which wellbore working parameters should be used, is also not known in advance. Therefore, the analysis and evaluation of the risks involved with multiple reservoir injection are difficult.

Bai et al. [14] derived an analytical solution for two-phase flows based on the work of Nordbotten et al. [17], and a solution was derived to designate the wellhead injection pressure. These authors characterized the risks of a reservoir using the ratio of the actual pressure of the fluid to the maximum allowable pressure. A higher ratio indicates that the corresponding reservoir is more dangerous. The reservoir that has the largest ratio is the weakest reservoir, which is also defined as the critical reservoir (CR). As the shortest slab in terms of the Cask principle, the CR actually constrains the maximum allowable wellhead injection pressure. Although the actual injection pressures are typically less than the maximum

allowable value, the injection flow rates can vary, which may lead to variation of CR's location. On such occasions, one cannot determine which layer is the CR because the downhole pressures and flow rates of all the reservoirs are initially unknown. Therefore, investigations of the effects of the injection parameters on the allocations of the total flow rates among multiple layers are extremely valuable.

This paper investigates the determination of CRs and their influencing factors during multireservoir CO_2 injection. For this purpose, the allocation percentage of the total flow rates among the multiple reservoir layers and the risk evaluation of the reservoirs must be simultaneously investigated. Such an investigation is expected to enrich the analysis and design methodologies for CO_2 injection operations. First, we outline the basic theory of the wellbore pressure and temperature. Then, a base case for determining the CR is presented. Next, we analyze the influences of the injection parameters and reservoir properties on the allocation percentage of the total flow rate, the reservoir risk, and the position of the CR. Finally, we summarize our main findings and conclude the study.

2. Fundamental Theory

To achieve the goal of this study, the coupling calculations for the flow and heat transfer of the wellbore and formation must be performed. Although various methods, including three-dimensional numerical simulations, could be employed, a semianalytical method developed by Bai et al. [14] and based on a fast, explicit numerical method and an analytical solution is used to calculate the wellbore flow and heat exchange between the wellbore and formations in this paper. The method is fast and can be applied successfully. In this method, the wellbore is discretized into a series of one-dimensional elements, and the model should include the following assumptions:

(1) One-dimensional flow with homogenous fluid is assumed in the vertical wellbore, and all the state variables and properties are assumed to be uniform at the same section.

(2) Only radial heat transfer is considered, and the temperature at each point is updated using Ramy's solution [18].

(3) The influence of the phase change on the fluid properties is not considered.

(4) All of the fluid properties should be constant within an element.

(5) The portion of the wellbore in the reservoir is simplified as an element node; that is, the variation in the state variables of the wellbore fluid is held constant in a reservoir.

The CO_2 pressure can be determined when the injection pressure at the wellhead is known; then, the fluid pressure P_{j+1} at the end point of the j-th well segment can be acquired from the following equation when P_j is already known:

$$P_{j+1} = P_j \left[1 + \frac{\Delta x_j \left(P_j^2 Mg/RT_j Z_j - \left(\gamma \overline{C}_j^2 RT_j/4r_0 \right) \left(Z_j/M \right) \right)}{\left(P_j^2 - \left(\overline{C}_j^2 RT_j/M \right) Z_j \right)} \right], \tag{1}$$

where $\overline{C}$ is the mass flow velocity of the wellbore cross section ($kg \cdot m^{-2} \cdot s^{-1}$), Δx is the discretized segment (m), g is the acceleration of gravity (m/s^2), r_0 is the inner radius of the tubing (m), M is the gas molar mass (kg/mol), R is the universal gas constant, γ is the coefficient of friction, Z is the compression factor obtained by solving the Peng-Robinson equation [19], and T is the thermodynamic temperature (K). The subscript j is used to number the discretized segments of the wellbore in the finite difference method.

As noted above, Ramy's analytical solution is used to obtain the CO_2 temperature of the wellbore. The details of the derivations are provided in the studies of Liu et al. [15] and Wu et al. [16], and the heat transfer between the wellbore and the surrounding earth is detailed in the study by Streit and Hillis [13].

The steady two-phase flow for the CO_2 flooding in the reservoir can be characterized by an equation proposed by Nordbotten et al. [17], with the assumption that a reservoir can be divided into CO_2-saturated and brine-saturated zones with a sharp interface. Obtaining an analytic solution from Nordbotten's equation is almost impossible. According to the derivation, by introducing two-phase mobility into the Darcy formula of a single-phase flow and assuming that the CO_2 plume is radially symmetric, as suggested by Wu et al. [20, 21] and Bai et al. [12], the mass flow rate C_i^r, which enters the i-th reservoir from the wellbore, can be expressed as follows:

$$C_i^r = 2\pi k_i B_i \rho_i \cdot \frac{P_{ki} - P_{0i}}{(1/\lambda_{ci}) \ln (R_{ci}/r_0) + (1/\lambda_{wi} - 1/\lambda_{ci}) + (1/\lambda_{wi}) \ln (R_{0i}/R_{\max i})}, \tag{2}$$

where P_0 is the initial formation pressure of the reservoir (Pa); P_k is the injection pressure on the wellface of the reservoir (Pa); R_0 is the maximum influence radius of the flow in the reservoir (m); R_c and $R_{\max}$ are the radii of the CO_2 plume at the bottom and top of the reservoir, respectively (m); k is the absolute permeability of the reservoir (m^2); B is the thickness of the reservoir (m); ρ is the density of the CO_2 (kg/m^3); and λ_c and λ_w are the mobility of CO_2 and the mobility of brine ($m \cdot s/kg$), which are defined as the ratios of their relative permeability to their fluid viscosity, that is, $\lambda_c = k_{rc}/\mu_c$ and $\lambda_w = k_{rw}/\mu_w$. Since the saturations of brine in the CO_2 and brine domains of a reservoir are zero and one, respectively, the relative permeabilities of k_{rc} and k_{rw} are both equal to one.

Moreover, three of the parameters in (2), R_0, and R_c, and $R_{\max}$, are used to describe the distributions of CO_2 and brine

in a reservoir. These parameters are time-dependent and can be calculated as follows:

$$R_0 = \sqrt{\frac{2.24kt}{\mu_w \varphi \left(\alpha_p + \beta_w\right)}} + R_{\max}, \tag{3a}$$

$$R_c = \sqrt{\frac{\lambda_w V^r(t)}{\lambda_c \varphi \pi B}}, \tag{3b}$$

$$R_{\max} = \sqrt{\frac{\lambda_c V^r(t)}{\lambda_w \varphi \pi B}}, \tag{3c}$$

where t is the injection time (s); $V^r(t)$ is the total flow into a reservoir during 0–t (m^3); φ is the reservoir porosity; α_p is the pore compressibility (m^2/N); β_w is the compressibility of brine (m^2/N); and μ_w is the viscosity of brine (kg/m/s).

According to the flow equilibrium conditions, the inflow of the section of the wellbore in the i-th reservoir is equal to the summation of the outflow into the next well segment and the corresponding reservoir [12]. Therefore, the following equation is obtained:

$$\overline{C}_i = \frac{2k_i B_i \rho_i}{r_0^2} \cdot \frac{P_{ki} - P_{0i}}{(1/\lambda_{ci}) \ln\left(R_{ci}/r_0\right) + (1/\lambda_{wi} - 1/\lambda_{ci}) + (1/\lambda_{wi}) \ln\left(R_{0i}/R_{\max i}\right)} + \frac{\rho_i}{\rho_{i+1}} \overline{C}_{i+1}. \tag{4}$$

When (4) is used for the bottom reservoir, the second term on the right-hand side disappears.

Typically, the site stability and the flow-rate target must also be satisfied and form the constraints during CO_2 injections. The wellbore constraints include the pressure and flow-rate constraints. The lower limit of the latter can be determined during the project-feasibility stage, whereas the upper limit requires each branch flow to meet the corresponding constraint conditions. Therefore, the complete wellbore constraints can be expressed as

$$\begin{aligned} P_{0i} + P_{bi} < P_{ki} \le \left[P_{ki}\right], \\ C_i^r \le \left[C_i^r\right], \end{aligned} \tag{5}$$

where P_b represents the capillary pressure (Pa); $[P_{ki}]$ is the maximum allowable pressure of the i-th reservoir (Pa), which is the formation-fracturing pressure multiplied by a synthetic design coefficient η; and $[C^r]$ is the available reservoir capacity (kg/s).

3. Example of the Shenhua CCS Demonstration Project

The Shenhua CCS demonstration project is the first fully implemented CCS project in China; the storage target of this project was set to 100,000 tons/year. A single injection well, which is referred to as ZSZ1, was drilled to a depth of 2,450 m, penetrating 21 reservoir-cap rock pairs, which were then combined and reduced to eight reservoir-cap rock units for analysis by Bai et al. [14]. From top to bottom, the geological formations include the Zhifang group, Heshanggou group, Liujiagou group, Shiqianfeng group, Shihezi group, Shanxi group, Taiyuan group, Benxi group, and Majiagou group. Table 1 lists the computational parameters of the reservoir-cap rock units from top to bottom. The other parameters, that is, the inner radius of the tubing r_0, pore compressibility α_p, brine compressibility β_w, CO_2 viscosity μ_c, and brine viscosity μ_w, were set to 31 mm, 4.5×10^{-10} m^2/N, 4.5×10^{-10} m^2/N, 88 kg/m/s, and 552 kg/m/s, respectively.

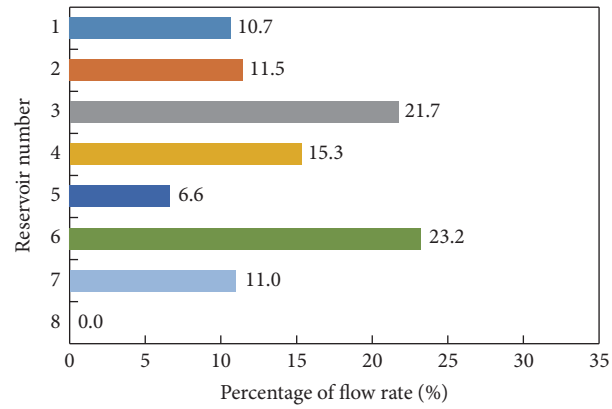

Figure 1: Flow-rate distribution among the reservoirs for the base case of the Shenhua CCS project.

As noted above, a forward analysis is employed in this study. Therefore, the parameters of the wellhead, such as the wellhead injection pressure and injection flow rate, must be prepared before the aforementioned method can be used to obtain the pressure and CO_2 injection flow rates of the reservoirs. Based on these values, the ratio $P_{ki}/[P_{ki}]$ can be obtained for the i-th reservoir. The synthetic design coefficient for obtained $[P_{ki}]$ is 0.8. The boundary conditions, that is, the injection pressure and injection rate at the wellhead, are 5 MPa and 4.63 kg/s, respectively, in the base case, which is consistent with the actual operational values at a certain injection stage. In addition, the calculated injection time is 3 years.

According to the distribution of the flow rates in the eight reservoirs plotted in Figure 1, the CO_2 flows are greater in the upper reservoirs under the given injection parameters. The flow rates of the upper four reservoirs account for 59.2% of the CO_2 flow, although the sixth reservoir has the largest flow rate, accounting for 23.2% of the total. Reservoirs 5, 7, and 8 comprise considerably lower percentages of the total flow rate.

The risk factors of all eight reservoirs, which are defined as the ratios of the actual pressures of the fluid P_{ki} to the maximum allowable pressures $[P_{ki}]$ at the entrances of the reservoirs, are shown in Figure 2. Reservoir 8 has the highest risk factor and is thus the CR. Bai et al. [14] found that a different reservoir was the CR when using different injection parameters. Hence, the CR is closely related to the injection

Table 1: Parameters of the reservoir-caprock units of the Shenhua CCS project.

Reservoir number	Thickness of reservoir (m)	Thickness of caprock (m)	Logging permeability ($\times 10^{-3}$ μm^2)	Logging porosity (%)	Fracturing pressure (MPa)	Formation pressure (MPa)
1	9	1699	2.81	10.6	35.29	17.45
2	5	57	5.47	12.4	37.53	17.89
3	40	191	1.431	9.7	38.95	20.15
4	8	43	6.58	12.9	42.60	21.43
5	4	119	5.99	12.6	47.00	22.94
6	26	114	2.738	12.5	43.47	23.1
7	8	52	5.1	11.9	46.03	23.84
8	12	178	0.039	5.2	45.68	22.75

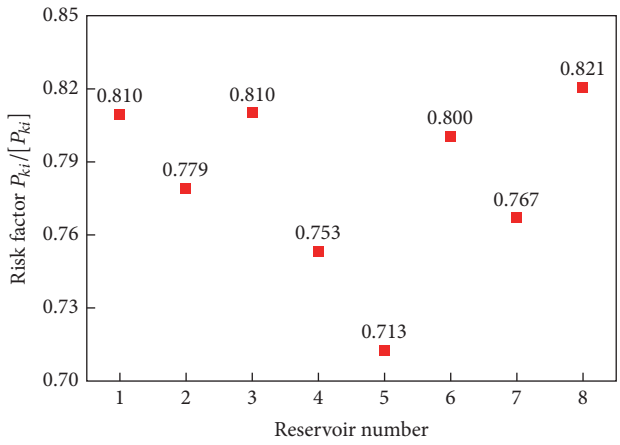

Figure 2: Risk factors of each reservoir for the base case of the Shenhua CCS project.

parameters. Because all the risk factors are less than 1.0, the given combination of injection parameters will not induce reservoir failure; the CR has a safety reserve of nearly 18%. In addition, Reservoir 8, which exhibits the minimum proportions of CO_2 entry, is the most dangerous reservoir, which indicates that the pressure might build up sharply at the wellface because of the poor injectivity under the given injection conditions.

4. Analysis of the Influencing Factors

Because the injection parameters are typically not constant during the actual injection operations, it is valuable to know how the risks and proportions of the flow rates in each reservoir depend on the injection conditions. Knowing whether the CR will shift because of the variations in the injection parameters is more important. In addition to these injection parameters, the characteristic parameters of the reservoirs are believed to be important influencing factors. The typical characteristic parameters of reservoirs include the reservoir thickness, porosity, permeability, initial formation pressure, and formation-fracturing pressure [2]. The two classes of factors, that is, the injection and characteristic factors, will be investigated in a subsequent study. The injection fluid is assumed to be pure CO_2, so the effects of impurities are not considered. Although the saturation of the fluid can significantly affect the distribution of the wellbore pressure and the wellhead pressure in particular, this factor will not change the CR [12]. Therefore, the effects of the characteristic physical parameters of the fluids will not be further investigated in this study.

4.1. Injection Parameters. In this subsection, we utilize the wellbore model and analysis method presented in the previous section. The main injection parameters of interest in this section are the injection pressure, injection flow rate and injection temperature. Ten injection cases are described in Table 2 based on combinations of these three parameters. The settings of the parameter values, which are chosen by considering the base case in the previous section and the actual injection history, are likely to be used in actual injection practices. Therefore, the results should provide valuable guidance for any subsequent injection operations during the Shenhua CCS project. The cases shown in Table 2 were designed with four targets, that is, determining the effect of variations in the injection pressures (Cases 1A to 1D), injection rates (Cases 1D to 1F), injection temperatures (Cases 1G to 1J), and combinations of the first two factors (Cases 1C, 1E, and 1G) on the percentages of the CO_2 inflows and the risks of each reservoir. All the designed parameter values ensure the safety of each reservoir because the target of this study is not the failure properties of the formations but the sensitivities of the CR to the parameters. The responses of the percentages of the CO_2 flow rates and the risk factors for each reservoir are illustrated in Figures 3 and 4, respectively.

Figure 3(a) shows that the proportion of CO_2 that flows into each reservoir varies with changes in the injection pressure under the given flow rates and temperatures at the wellhead. With greater injection pressures, the inflows into Reservoirs 1–5 increase monotonically, the inflows into Reservoir 6 initially increase and then decrease, and the inflows into Reservoirs 7-8 gradually decrease. These variation trends indicate that a greater injection pressure causes more CO_2 to enter the upper reservoirs because of the increase in the fluid pressure at the wellbores in the reservoirs and the constant total flux at the wellheads. Figure 4(a) indicates that the reservoir risk also increases due to the increased injection pressure. More importantly, the risk-increasing trends of the upper

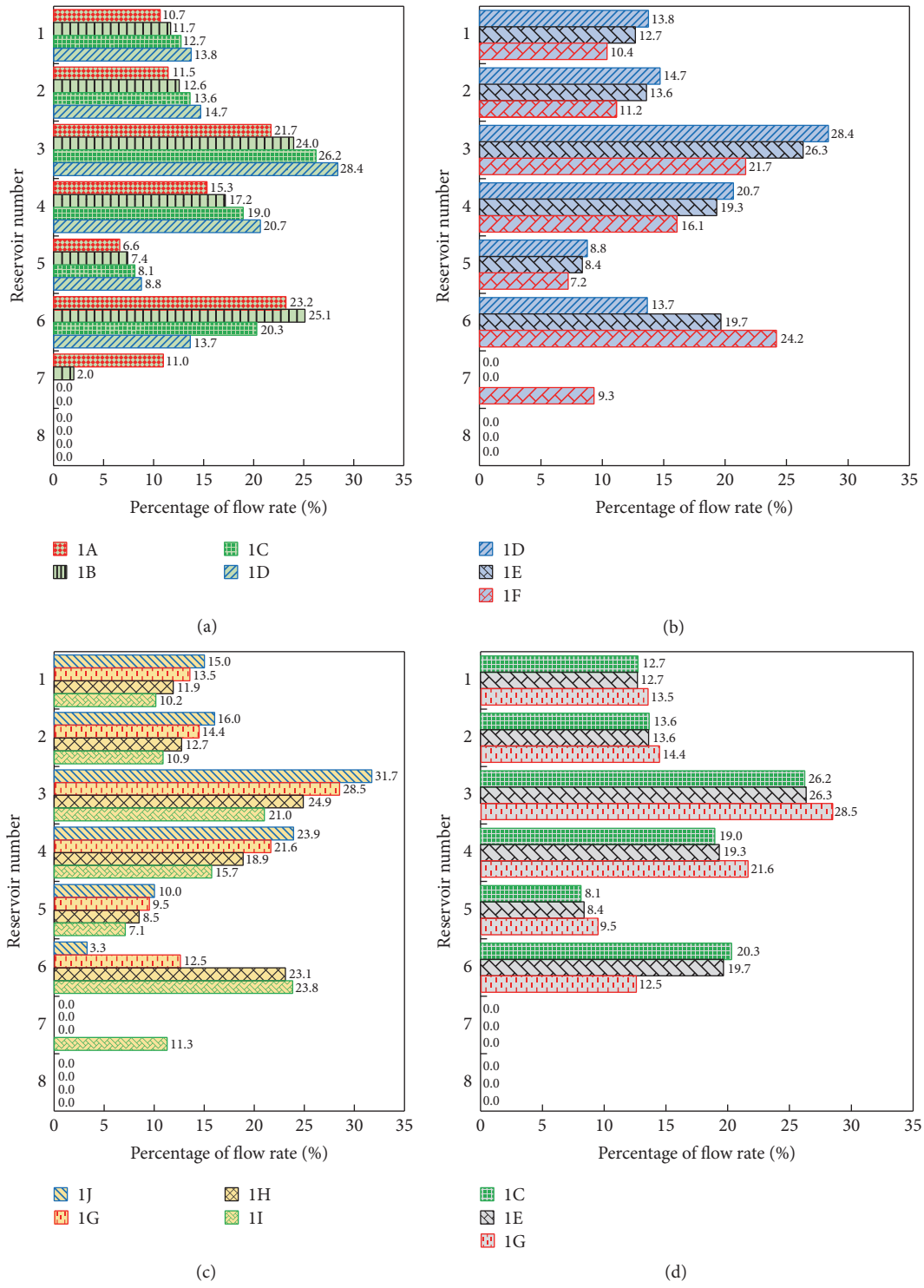

FIGURE 3: Distributions of the flow rates that correspond to the different injection parameters at the wellhead of the Shenhua CCS project. (a), (b), and (c) are the results for different injection pressures, flow rates, and temperatures, respectively. (d) shows the investigation of the influences of simultaneous changes of the injection pressures and flow rate.

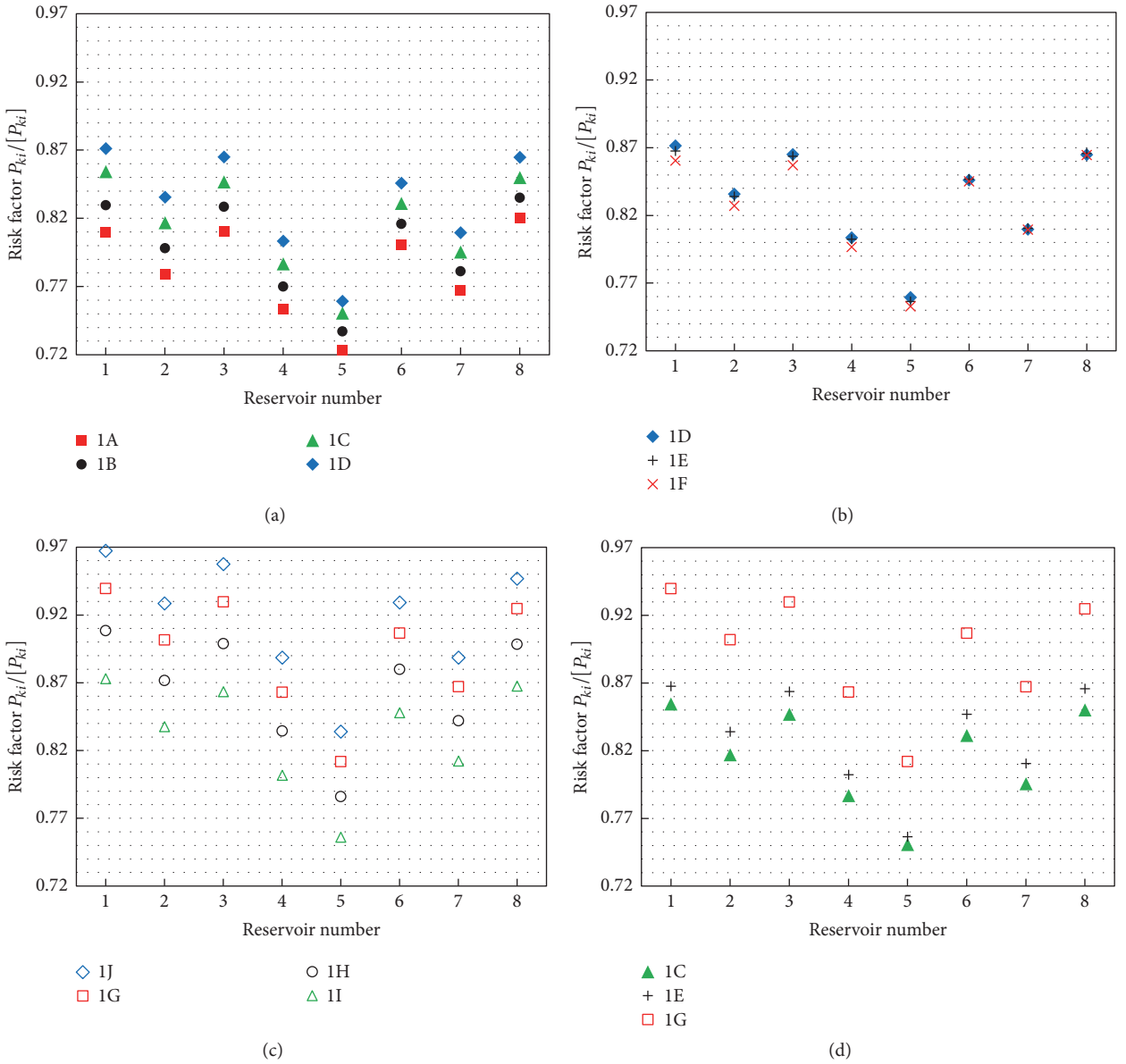

Figure 4: Risk factors of each reservoir which correspond to the different injection parameters at the wellhead of the Shenhua CCS project. (a), (b), and (c) are the results for the different injection pressures, flow rates, and temperatures, respectively. (d) Investigation of the influences of simultaneous changes of the injection pressures and flow rates.

Table 2: Injection parameters for the described cases of the Shenhua CCS project.

Case	Injection pressure (MPa)	Injection flow rate (kg/s)	Injection temperature of CO_2 (°C)
1A	5	4.63	−5
1B	6	4.63	−5
1C	7	4.63	−5
1D	8	4.63	−5
1E	8	5	−5
1F	8	6	−5
1G	10	6	−5
1H	10	6	5
1I	10	6	15
1J	10	6	−15

Table 3: Characteristic parameters of the reservoirs in the conceptual engineering model.

Reservoir number	Thickness of reservoir (m)	Thickness of caprock (m)	Logging permeability ($\times 10^{-3}$ μm^2)	Logging porosity (%)	Fracturing pressure (MPa)	Formation pressure (MPa)
1	10	1390	6	12	35	15
2	10	190	5	11	38	17
3	10	190	4	10	41	19
4	10	190	3	9	44	21

reservoirs are more dramatic than those of the lower reservoirs. When the injection pressure reaches 7.0 MPa, the CR transfers from Reservoir 8 to Reservoir 1, indicating that the injection pressure can control the overall risks of the reservoirs and that concentrating CO_2 in the upper reservoirs causes the CR to shift to the top reservoir because of the increased injection pressure.

Figure 3(b) shows the variations of the distributions of the CO_2 flow rates among the reservoirs with increases in the injection flow rates when the injection pressure and injection temperature are known. In contrast to Figure 3(a), a higher total injection flow rate increases the proportion of CO_2 that flows into the lower reservoirs. This is mainly because the pressure attenuation increases with the injection flow rate such that the flows into the upper reservoirs are reduced. Moreover, as shown in Figure 4(b), the risks of all the reservoirs gradually decrease from Case 1D to Case 1F, and the CR shifts back to Reservoir 8, which differs from the results presented in Figure 4(a). However, the risk reductions of these reservoirs are relatively small, particularly for the lower reservoirs, even when their flow rates are increased. Thus, the injection flow rate has a smaller impact on the risk of a reservoir than the injection pressure does, and both parameters have larger impacts on the risks of the upper reservoirs than on the risks of the lower reservoirs.

As the injection temperature of CO_2 increases, the variation trends of the flow rates in each layer become opposite to those induced by the increases in the injection pressure, despite agreeing well with those shown in Figure 3(b) for the gradually increasing concentrations of CO_2 in the upper reservoirs, as shown in Figure 3(c). Similarly, Figure 4(c) indicates that the changes in the reservoir risks are approximately opposite to those in Figure 4(a). This decrease in the reservoir risk is likely induced by a drop in the viscosity, which can accelerate the transport of fluids and lead to a partial dissipation of pressure because of the increasing injection temperature. Furthermore, Reservoir 1 remains the CR, even though the reservoir risk decreases with the increasing injection temperature.

Given the synchronous variations in injection pressures and flow rates, the injection proportion of each reservoir remains almost invariant, except for that of Reservoir 6, which exhibits a 7.5% decrease in Case 1G, as shown in Figure 3(d). However, the risks of all the reservoirs in Figure 4(d) increase significantly, but Reservoir 1 remains the CR. In combination with the results shown in Figures 4(a) and 4(b), the injection pressure is shown to predominantly control the overall risks of the reservoirs, and the injection flow rate is shown to be able to affect the position of the CR to a certain extent.

4.2. Characteristic Parameters of the Reservoirs

4.2.1. Parameter Settings. The injectivity of the reservoir and the downhole limitations of the injection pressure depend on the reservoir's characteristic parameters; variations in these parameters can affect the intake percentages and risks of each reservoir. For a CCS project, these parameters are typically considered to be constant. The objective of this section is to determine the effects of these parameters; therefore, the assumed parameters rather than the experimental parameters of the Shenhua CCS project are employed to conduct a parameter sensitivity analysis. A conceptual engineering model that contains four reservoir-cap rock units with a single injection well that penetrates 2,000 m underground is established. The formations in the conceptual model, from top to bottom, are as follows: Cap rock 1, Reservoir 1, Cap rock 2, Reservoir 2, Cap rock 3, Reservoir 3, Cap rock 4, and Reservoir 4. The depths of the bottoms of these formations are 1390 m, 1400 m, 1590 m, 1600 m, 1790 m, 1800 m, 1990 m, and 2000 m, respectively. The basic characteristic parameters of the reservoirs are listed in Table 3, and the parameters of the wellbores are the same as those for the Shenhua CCS project. For the base case, the wellhead injection pressure, injection flow rate, and injection temperature of CO_2 are set to 10 MPa, 4 kg/s, and −5°C, respectively. Five cases with the same initial states as the base case (Table 3) are designed to study the influence of each reservoir's parameters. The injection time is set to ten years.

4.2.2. Influence of the Formation-Fracturing Pressure. As presented above, the concept of the CR depends on the $P_{ki}/[P_{ki}]$ ratio. $[P_{ki}]$ is typically obtained from the formation-fracturing pressure multiplied by the synthetic design factor, which is smaller than 1.0. In this conceptual model, the synthetic design factor is set to 0.6. Therefore, $[P_{ki}]$ represents the intrinsic ability of a formation to resist damage and is a decisive factor in determining the risk of a reservoir and the position of the CR, which will be investigated first. Five groups of fracturing pressures are designed and listed in Table 4. In Cases 2B and 2C, the formation-fracturing pressures of Reservoirs 2 and 3, respectively, are obtained by slightly decreasing the corresponding values in Case 2A.

Table 4: Cases with different formation-fracturing pressures (MPa).

Reservoir number	2A (base case)	2B	2C	2D	2E
1	35	35	35	35.5	36
2	38	37	38	38.5	39
3	41	41	40	41.5	42
4	44	44	44	44.5	45

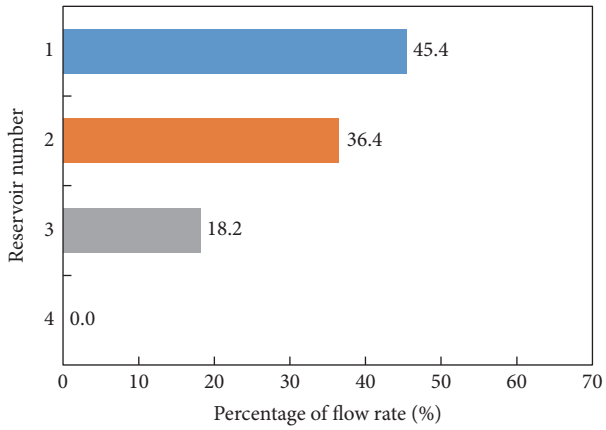

Figure 5: Flow-rate distribution of a conceptual model with the corresponding parameters of the formations in Table 3; the injection pressure, flow, and temperature are 10 MPa, 4 kg/s, and −5°C, respectively.

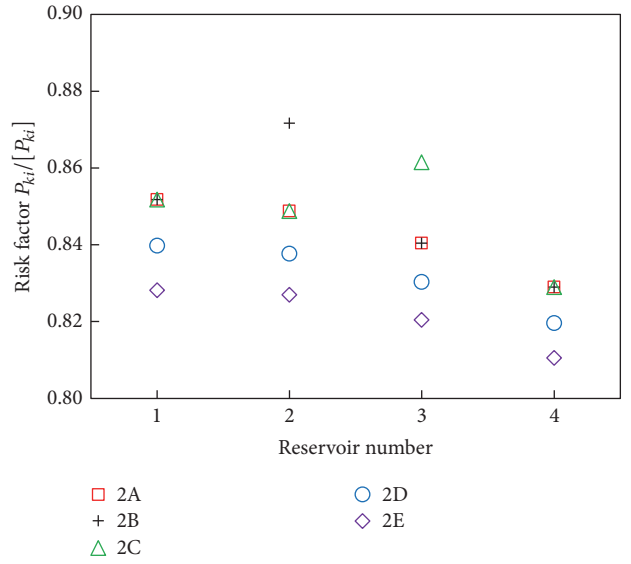

Figure 6: Variations in the risk factors of the reservoirs at different formation-fracturing pressures for the conceptual engineering model.

Therefore, the effect of the decrease in the formation-fracturing pressure of a single reservoir on the intake percentage and the risk of each reservoir can be investigated by comparing the results from Cases 2A to those of 2C. In Cases 2D and 2E, the fracturing pressures of all the reservoirs increased by 0.5 and 1.0 MPa, respectively. Using these results, the effects of a synchronous increase in the formation-fracturing pressures can be studied. The percentages of the inflows and the risks of each reservoir in these five cases are illustrated in Figures 5 and 6, respectively.

The formation-fracturing pressure does not influence the CO_2 pressure or injectivity. Therefore, modifying the formation-fracturing pressures does not alter the proportion of CO_2 that flows into each reservoir. As shown in Figure 5, the majority of CO_2 enters the upper two reservoirs. In contrast, variations of the formation-fracturing pressure considerably affect the risks of the reservoirs (Figure 6) and can cause the CR to shift. A comparison of the results of Cases 2A, 2B, and 2C indicates that when the fracturing pressure of only one reservoir formation is reduced, the risk of this reservoir immediately increases, such that this reservoir will become the CR when the formation-fracturing pressure decreases to a certain value. Furthermore, an identical increment in the formation-fracturing pressures of all the reservoirs should improve the safety of the reservoirs, and the reservoir with the smallest fracturing pressure will exhibit the largest decrease in risk. Similarly, increasing all the reservoirs' formation-fracturing pressures should decrease the risks of the reservoirs without altering the position of the CR.

4.2.3. Influence of the Initial Formation Pressure. In engineering practices, the initial formation pressure is used to determine the lower limit of the injection pressure of the reservoir. Because the injection pressure is typically considerably higher than the initial formation pressure, variations in the initial formation pressure will not affect the reservoir risk directly but will affect the intake percentage of each reservoir. As discussed above, the uppermost reservoir is the CR for the original set of parameters used in this study. Because the pressure at this reservoir can be calculated directly from the wellhead conditions and is not related to the proportion of the CO_2 inflow, the uppermost reservoir will remain the CR with the use of the original set of parameters. To further investigate these characteristics, another base case in which the CR is not the uppermost reservoir must be constructed, and the initial case can then be used as a reference to investigate the effects of varying the initial formation pressure.

Because the formation-fracturing pressure can affect the position of the CR considerably, directly changing its value allows the construction of a reference case. Therefore, two scenarios (i.e., S-1 and S-2) with two sets of formation-fracturing pressures are presented, and the settings of the formation-fracturing pressures of S-1 and S-2 are the same as those of Cases 3A and 3C, respectively, as shown in Table 4. Five different initial formation pressures for each scenario are provided in Table 5.

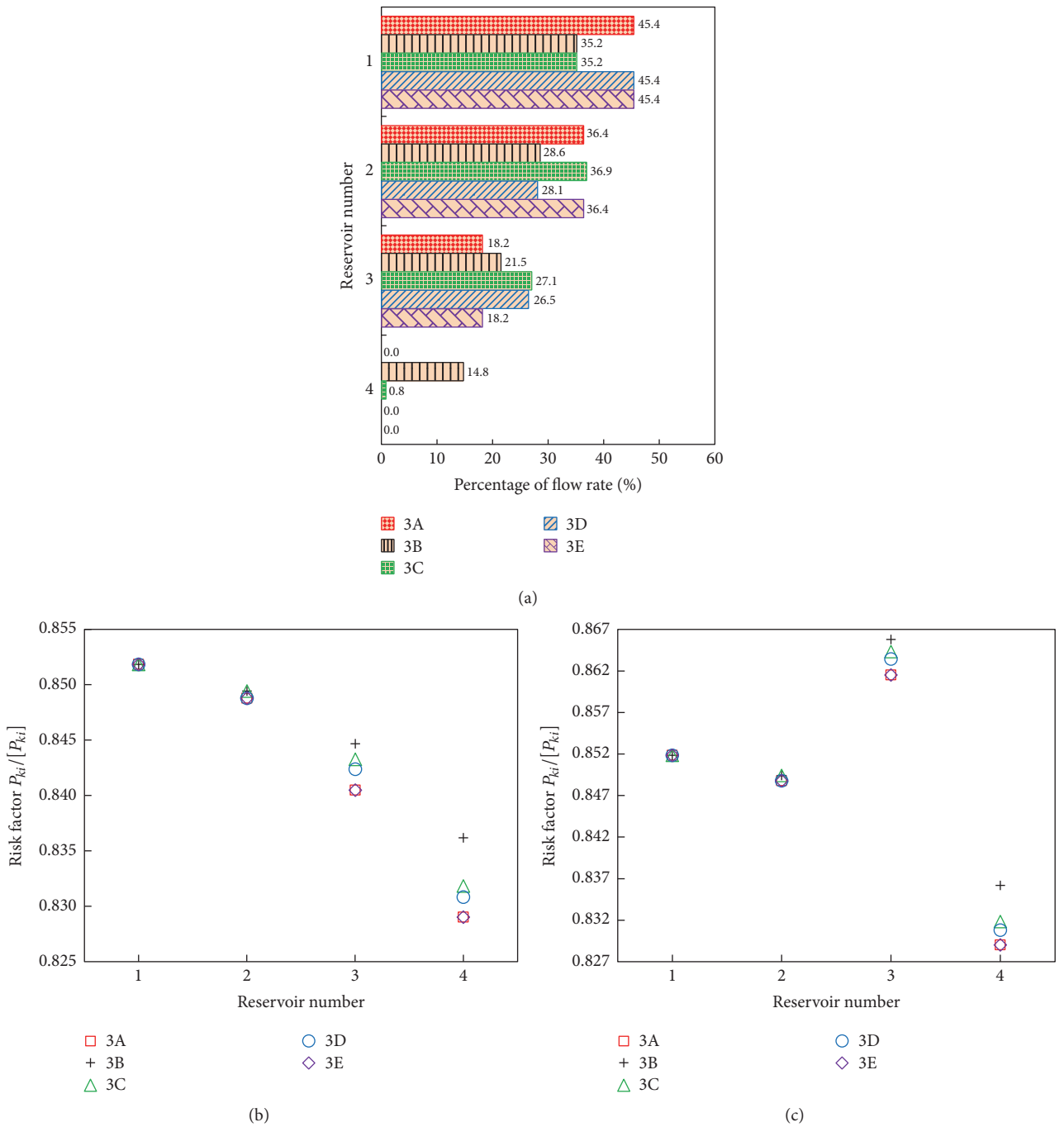

FIGURE 7: Proportions of the inflows (a) and risk factors of each reservoir under different initial formation pressures for the two scenarios of the conceptual engineering model. (b) and (c) are the risk-factor results for Scenarios S-1 and S-2, respectively.

As noted above, the proportion of CO_2 that flows into each reservoir is not related to the formation-fracturing pressure. The distributions of the flow rates among the reservoirs in S-1 and S-2 shown in Figure 7(a) are identical. Overall, when the initial formation pressure of a layer increases, the injection proportion of this layer decreases, whereas the flow rate that enters the layer beneath also increases. The inflow proportion for the uppermost reservoir changes only when its initial formation pressure changes. However, the initial formation pressures of the first and second reservoirs affect the inflow proportion of the second reservoir. The remaining inflow proportions can be deduced via an analogy; that is, the percentage of CO_2 that enters a reservoir is related to the variation of the initial formation pressure of the reservoir itself and its upper reservoirs.

As the initial formation pressure increases, the risks of the reservoirs below the uppermost reservoir also increase, whereas the risk of the uppermost reservoir remains constant.

Table 5: Five cases with different initial formation pressures (MPa).

Reservoir number	3A (base case)	3B	3C	3D	3E
1	15	17	17	15	15
2	17	19	17	19	17
3	19	21	19	19	21
4	21	23	21	21	21

Table 6: Five cases with different reservoir thicknesses (m).

Reservoir number	4A (base case)	4B	4C	4D	4E
1	10	20	20	10	10
2	10	20	10	20	10
3	10	20	10	10	20
4	10	20	10	10	10

Table 7: Five cases with different reservoir logging permeabilities ($\times 10^{-3}$ μm^2).

Reservoir number	5A (base case)	5B	5C	5D	5E
1	6	12	12	6	6
2	5	10	5	10	5
3	4	8	4	4	8
4	3	6	3	3	3

Table 8: Five cases with different reservoir logging porosities (%).

Reservoir number	6A (base case)	6B	6C	6D	6E
1	12	24	24	12	12
2	11	22	11	22	11
3	10	20	10	10	20
4	9	18	9	9	9

Moreover, the initial formation pressure has a greater effect on the lower reservoirs than on the upper reservoirs, as shown in Figures 7(b) and 7(c). A comparison between the five cases of the two scenarios indicates that changes in the initial formation pressures have greater effects on the risks of the upper reservoirs than on the risks of the lower reservoirs. Reservoirs 1 and 3 are the CRs in S-1 and S-2, respectively. Thus, changes in the initial formation pressures also influence the position of the CR. In S-1, when the initial formation pressure of Reservoir 1 continues to increase, the risks of the lower reservoirs increase, and both Reservoirs 2 and 3 have the potential to become the CR. In S-2, when the initial formation pressure of Reservoir 1 or Reservoir 2 decreases to a certain value, then the risk of Reservoir 3 decreases and Reservoir 1 becomes the CR. Thus, when the first layer is not the CR, the risk of the CR can be reduced by decreasing the initial formation pressure of the upper reservoirs, which can help improve the safety and injectivity of the target site.

4.2.4. Influences of the Thickness, Permeability, and Porosity of the Reservoir. The thickness, permeability, and porosity of the reservoirs affect the capacity and injectivity of the reservoirs, which then affect the inflow and CO_2 pressure in the wellbore, which is similar to the role of the initial formation pressure. Therefore, in this section, the aforementioned scenarios, S-1 and S-2, are used as the working models. The cases in Tables 6–8 were designed to investigate the effects of these three parameters, respectively. Changing the parameters of the last reservoir alone does not affect any of the results for the entire wellbore; hence, only the parameter sensitivities of the first three reservoirs are investigated.

Figure 8(a) shows the proportion of CO_2 injected into each reservoir, considering the different reservoir thicknesses. The results in Figures 7(a) and 8(a) illustrate that as the thickness of a reservoir increases, the CO_2 inflows into its upper reservoirs remain unchanged, whereas those of the reservoir itself and its lower reservoirs increase and decrease, respectively. As shown in Figures 8(b) and 8(c), an increase in the thickness of a single reservoir can effectively reduce the risks of its lower reservoirs without affecting those of its upper reservoirs, which is similar to the decreasing effect of the initial formation pressure. Therefore, the risk of the first reservoir is always fixed, regardless of whether the thickness of the reservoir varies. Moreover, increasing the thicknesses of the upper reservoirs to reduce the reservoir risk is significantly more effective than increasing the thicknesses of the lower reservoirs. In Cases 4B and 4C of S-2, the CR shifts from Reservoir 3 to Reservoir 1, which can effectively improve the safety of the wellbore and verify the conclusion that the CR might shift with changes in the formation-fracturing pressure. Additionally, the results for Cases 4B and 4C are the same in each of the three subpanels of Figure 8, which does not mean that doubling the thickness of Reservoir 1 produces the same effect as scaling up the thicknesses of all the reservoirs at the same time. This phenomenon occurs because the flow rate into Reservoir 1 accounts for 94% of the total flow after scaling up its thickness by one under the given injection conditions, and the remaining flow rate does not satisfy the capacity of the lower reservoir. In other words, when the total injection flow rate is adequate, the differences between the results of Cases 4B and 4C will clearly manifest themselves.

The scheme for generating the cases used to examine the reservoir permeability is the same as that used for the reservoir thicknesses. As shown in Figure 9, the influence of the permeability of the reservoir on the distribution of the flow rates and the risks of the reservoirs is nearly the same as that of the thickness of the reservoir, as shown in Figure 8, because the inflow of a reservoir, as expressed by (2), is proportional to the thickness and permeability of the reservoir. Therefore, we do not describe Figure 9 in further detail. However, subtle differences do exist in the flow-rate distributions and risks of the results shown in Figures 8 and 9 for the two scenarios. In short, the permeability has less significant effects than the thickness of the reservoirs.

Figure 10 shows the results when considering different reservoir porosities. The distributions of the flow rates and

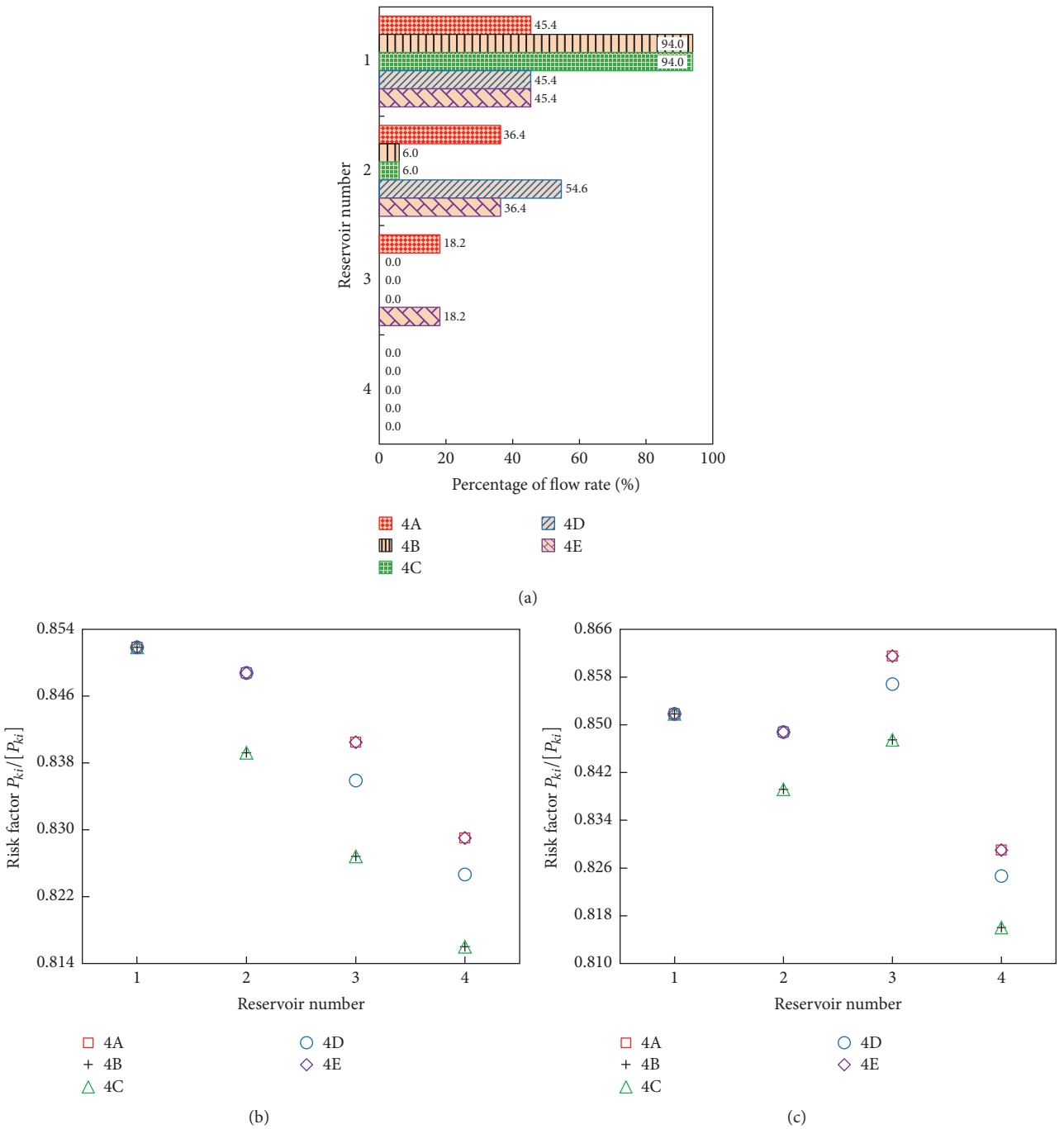

FIGURE 8: Proportions of the inflows (a) and risk factors of each reservoir for different reservoir thicknesses for the two scenarios of the conceptual engineering model. (b) and (c) are the risk-factor results for Scenarios S-1 and S-2, respectively.

risks of the reservoirs for each case agree well with each other. Thus, the effect of the variations in porosity can be neglected.

5. Conclusions

This paper presented a systematic study on the key issues that arise from multiple CO_2 injections during CCS projects, namely, the distributions of the flow rates among the reservoirs, the CRs, and their influencing factors. Understanding these issues is essential for both pressure design and field operations at wellheads. The calculation methods and programs were based on those in our previous work. Some specific conclusions of the study are given as follows.

(1) Assuming that all the reservoirs had identical properties, including thickness, porosity, and permeability, the

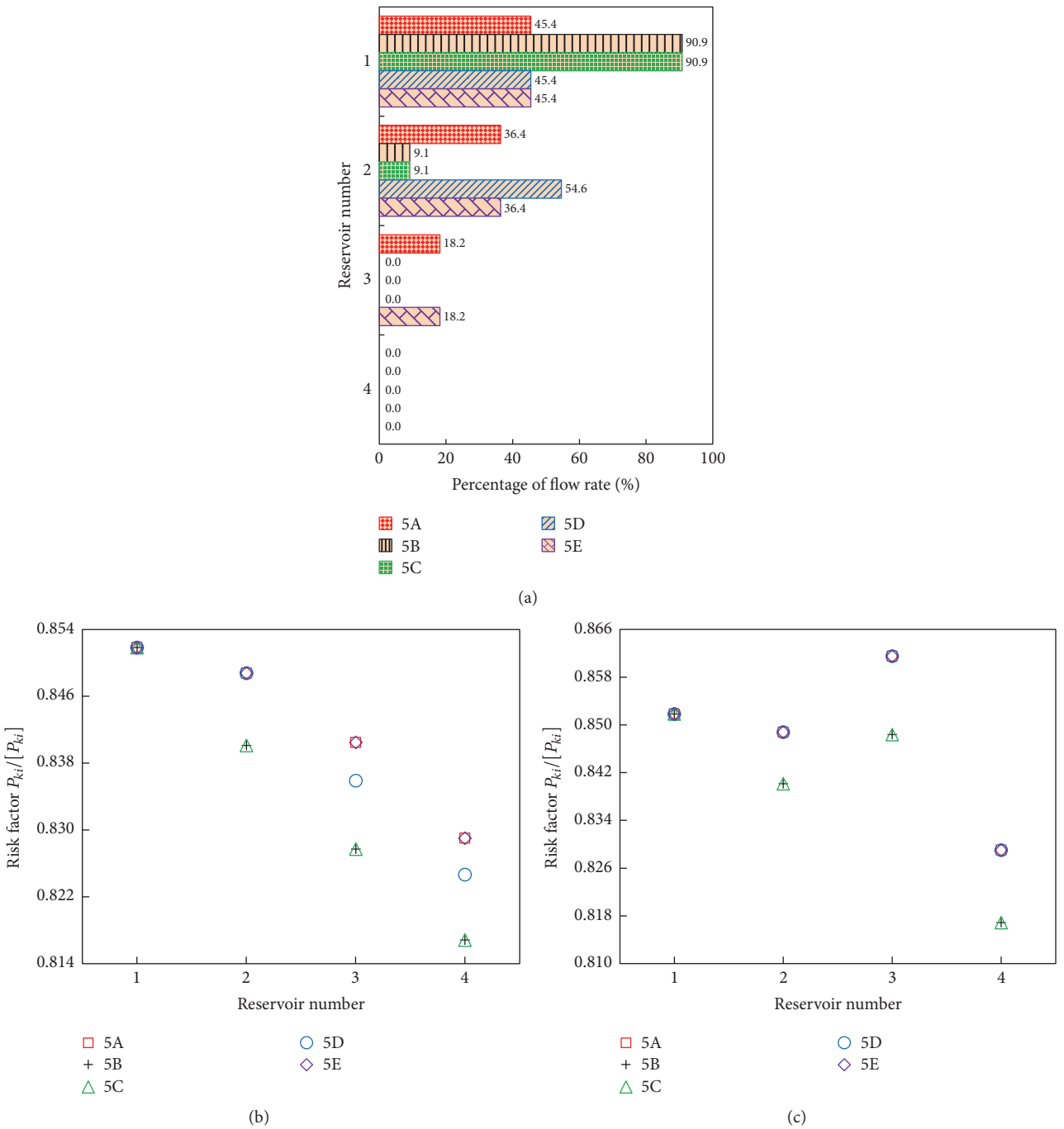

FIGURE 9: Proportions of the inflows (a) and risk factors of each reservoir for different reservoir permeabilities for the two scenarios of the conceptual engineering model. (b) and (c) are the risk-factor results for Scenarios S-1 and S-2, respectively.

injected fluid was mainly distributed in the upper reservoirs, and less CO_2 entered the lower reservoirs. This trend mainly occurred because deeper reservoirs have greater formation pressure; therefore, high formation pressures require higher injection pressures to maintain injectivity.

(2) The risk of the reservoir was mainly controlled by the injection pressure and the formation-fracturing pressure and was minimally related to the inflow of CO_2. Therefore, a reservoir could still be the CR even when the flow rate of CO_2 into that reservoir is close to zero.

(3) The injection parameters at the wellhead considerably affected the flow-rate distributions and risks of the reservoirs. More CO_2 entered the upper reservoirs than the lower reservoirs with increasing injection pressure (or decreasing injection rate). Moreover, the risks of all the reservoirs increased, and the risk-increasing trend of the upper reservoirs was

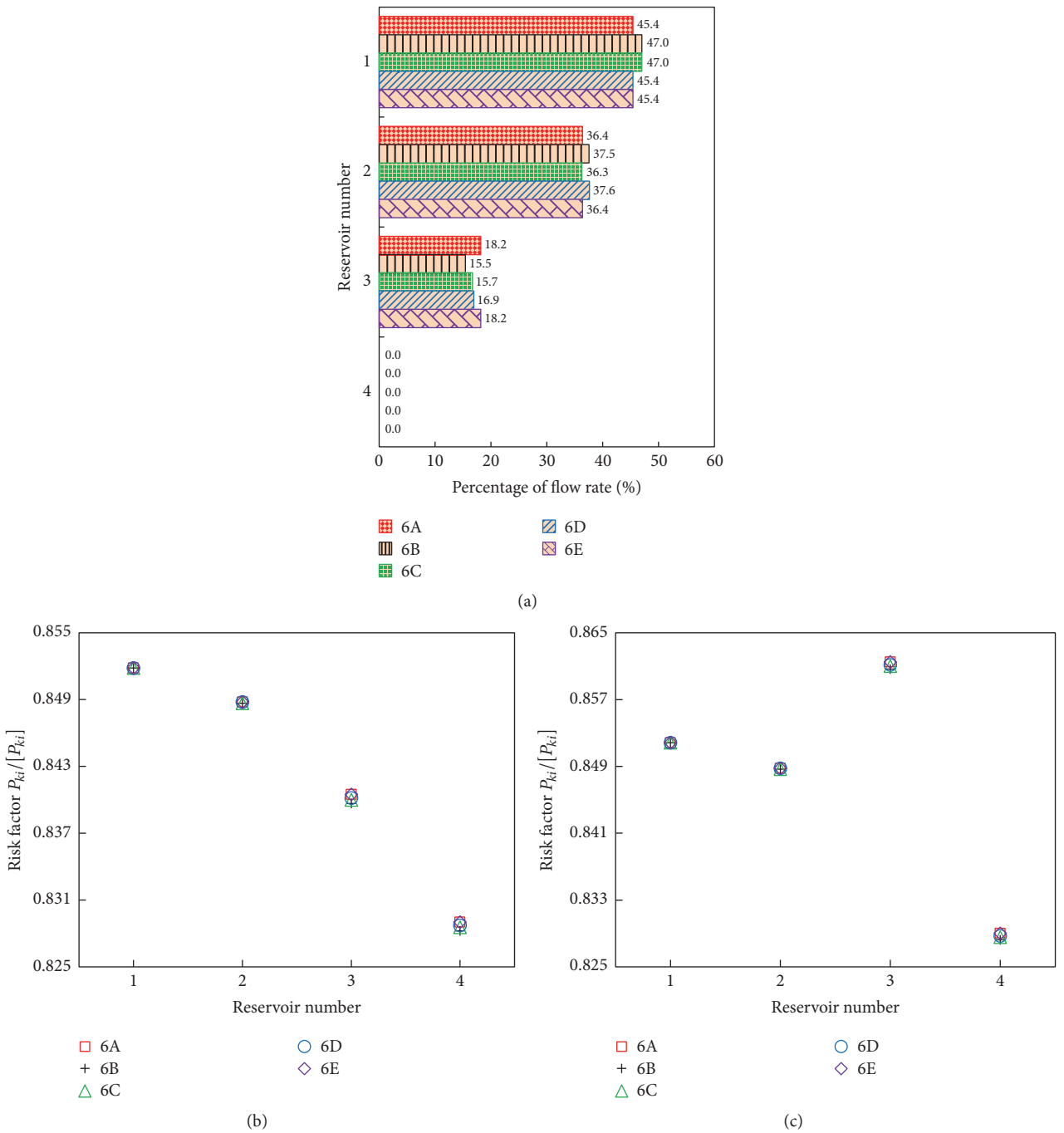

FIGURE 10: Proportions of the inflows (a) and risk factors of each reservoir for different reservoir porosities for the two scenarios of the conceptual engineering model. (b) and (c) are the risk-factor results for Scenarios S-1 and S-2, respectively.

notably greater than that of the lower reservoirs. Because the extent of the variation in each reservoir was different, the CR could shift. This result demonstrates that the injection pressure controls the overall risk level of the reservoir and the flow-rate distribution among the reservoirs can control the position of the CR. The CO_2 injection temperature had a similar effect as the injection flow rate, but the fluid injection temperature had no effect on the position of the CR.

(4) Although the formation-fracturing pressure does not affect the flow-rate distribution, it is one of the key factors for determining the reservoir risk and CR. Decreasing the formation-fracturing pressure increased the reservoir risk and cause the CR to shift. When the formation-fracturing pressures of all the reservoirs were decreased by the same factor, the risk of each reservoir increased equally without changing the CR. Under a constant flow rate, variations in

the reservoirs' porosities had a minimal effect on the flow-rate distribution and the reservoir risk. The thickness and permeability had similar effects on the flow-rate distributions and reservoir risks. For a specific reservoir, the flow rate increased with increasing thickness or permeability, and the flow rates of the lower reservoirs simultaneously decreased, whereas the flow rates of the upper reservoirs remained unchanged. Furthermore, only the risks of the lower reservoirs decreased with increases in these two parameters; therefore, the CR can shift to another reservoir. The initial formation pressure had the opposite effect as the reservoir thickness. Therefore, certain reservoirs can be selectively reformed according to their risks to decrease these risks and adjust the position of the CR, which can effectively improve the injection safety and utilization efficiency of the reservoirs.

(5) The injection flow rates notably influenced the flow-rate distribution. The position of the CR and injection flow rate may vary in actual CO_2 injection processes. The design of the maximum allowable wellhead injection pressure should consider multiple flow-rate scenarios to reduce uncertainties and to improve the reliability of the project.

(6) The results obtained from our investigations of the influence of the injection parameters on the flow-rate distributions and reservoir risks in the case study of the Shenhua CCS demonstration project can be used to guide subsequent injection operations. This research was based on a vertical wellbore that penetrated a number of reservoirs. Although the results for horizontal and inclined wells may be similar, further research on these topics is still required.

Conflicts of Interest

The authors declare that they have no conflicts of interest.

Acknowledgments

This work was sponsored by the International Science & Technology Cooperation Program of China (S2016G9005) under the cooperation framework of the US-China Clean Energy Research Center (CERC).

References

[1] S. Bachu, "CO_2 storage in geological media: role, means, status and barriers to deployment," *Progress in Energy and Combustion Science*, vol. 34, no. 2, pp. 254–273, 2008.

[2] S. Bachu, "Screening and ranking of sedimentary basins for sequestration of CO2 in geological media in response to climate change," *Environmental Geology*, vol. 44, no. 3, pp. 277–289, 2003.

[3] IPCC, *Climate Change 2014: Mitigation of Climate Change. Contribution of Working Group III to the Fifth Assessment Report of the Intergovernmental Panel on Climate Change*, Cambridge University Press, Cambridge, UK, 2014.

[4] IPCC., *IPCC special report on carbon dioxide capture and storage*, Cambridge University Press, Cambridge, UK, 2005.

[5] X. C. Li, Y. F. Liu, B. Bai, and Z. Fang, "Ranking and screening of CO_2 saline aquifer storage zones in China," *Chinese Journal of Rock Mechanics and Engineering*, vol. 25, no. 5, pp. 963–968, 2006 (Chinese).

[6] K. Michael, A. Golab, V. Shulakova et al., "Geological storage of CO_2 in saline aquifers—a review of the experience from existing storage operations," *International Journal of Greenhouse Gas Control*, vol. 4, no. 4, pp. 659–667, 2010.

[7] H. Kongsjorden, O. Karstad, and T. A. Torp, "Saline aquifer storage of carbon dioxide in the Sleipner project," *Waste Management*, vol. 17, no. 5-6, pp. 303–308, 1998.

[8] Z. Li, M. Dong, S. Li, and S. Huang, "CO_2 sequestration in depleted oil and gas reservoirs—caprock characterization and storage capacity," *Energy Conversion and Management*, vol. 47, no. 11-12, pp. 1372–1382, 2006.

[9] J. Underschultz, C. Boreham, T. Dance et al., "CO_2 storage in a depleted gas field: an overview of the CO2CRC Otway Project and initial results," *International Journal of Greenhouse Gas Control*, vol. 5, no. 4, pp. 922–932, 2011.

[10] X. Wu, "Shenhua group's carbon capture and storage (CCS) demonstration," *Mining Report*, vol. 150, no. 1-2, pp. 81–84, 2014.

[11] J. Rutqvist, J. Birkholzer, F. Cappa, and C.-F. Tsang, "Estimating maximum sustainable injection pressure during geological sequestration of CO_2 using coupled fluid flow and geomechanical fault-slip analysis," *Energy Conversion and Management*, vol. 48, no. 6, pp. 1798–1807, 2007.

[12] B. Bai, X. Li, H. Wu, Y. Wang, and M. Liu, "A methodology for designing maximum allowable wellhead pressure for CO2 injection: application to the Shenhua CCS demonstration project, China," *Greenhouse Gases: Science and Technology*, vol. 7, no. 1, pp. 158–181, 2017.

[13] J. E. Streit and R. R. Hillis, "Estimating fault stability and sustainable fluid pressures for underground storage of CO2 in porous rock," *Energy*, vol. 29, no. 9-10, pp. 1445–1456, 2004.

[14] B. Bai, X. Li, M. Liu, L. Shi, and Q. Li, "A fast explicit finite difference method for determination of wellhead injection pressure," *Journal of Central South University*, vol. 19, pp. 3266–3272, 2012.

[15] M. Liu, B. Bai, and X. Li, "A unified formula for determination of wellhead pressure and bottom-hole pressure," *Energy Procedia*, vol. 37, pp. 3291–3298, 2013.

[16] H. Wu, B. Bai, M. Liu, and X. Li, "The equivalent density method to estimate the wellbore pressure of CO2 well," *Special Oil and Gas Reservoirs*, vol. 22, pp. 114–117, 2015.

[17] J. M. Nordbotten, M. A. Celia, and S. Bachu, "Injection and storage of CO2 in deep saline aquifers: Analytical solution for CO2 plume evolution during injection," *Transport in Porous Media*, vol. 58, no. 3, pp. 339–360, 2005.

[18] H. J. Ramey, "Wellbore heat transmission," *Journal of Petroleum Technology*, vol. 140, no. 4, pp. 427–435, 1962.

[19] D. Y. Peng and D. B. Robinson, "A new two-constant equation of state," *Industrial and Engineering Chemistry Fundamentals*, vol. 15, no. 1, pp. 59–64, 1976.

[20] H. Wu, B. Bai, X. Li, S. Gao, M. Liu, and L. Wang, "An explicit integral solution for pressure build-up during CO2 injection into infinite saline aquifers," *Greenhouse Gases: Science and Technology*, vol. 6, no. 5, pp. 633–647, 2016.

[21] H. Wu, B. Bai, X. Li, M. Liu, and Y. He, "An explicit finite difference model for prediction of wellbore pressure and temperature distribution in CO2 geological sequestration," *Greenhouse Gases: Science and Technology*, vol. 7, no. 2, pp. 353–369, 2017.